Biomimetic synthesis of aragonite superstructures using hexamethylenetetramine

Long Chen [a,b,c], Fangzhi Huang [a], Shikuo Li [a], Yuhua Shen [a,*], Anjian Xie [a,*], Jian Pan [c],
Yaping Zhang [a], Yan Cai [a]

[a] School of Chemistry and Chemical Engineering, Anhui University, Hefei 230039, PR China
[b] Department of Chemistry, Huangshan University, Huangshan 245041, PR China
[c] Post-Doctoral Scientific Research Workstation, HuangShan NOVEL Co. Ltd, Huangshan 245061, PR China

ARTICLE INFO

ABSTRACT

In this paper, biomimetic synthesis of aragonite superstructures using a low molecular weight organic-hexamethylenetetramine (HMT) as an additive in the presence of CO_2 supplied by an ammonium carbonate $((NH_4)_2CO_3)$ diffusion method at room temperature was studied. The products were characterized by scanning or transmission electron microscopy, Fourier transform infrared (FT-IR) spectroscopy, X-ray powder diffractometry, and selected area electron diffraction. The results showed the aragonite superstructures especially dumbbell-flower-like ones were obtained. The formation process of calcium carbonate $(CaCO_3)$ in HMT aqueous solution was investigated, suggesting that the products transformed from calcite to vaterite primarily, and then changed into a mixture of aragonite and calcite with an increase of reaction time. The formation mechanism of $CaCO_3$ in HMT solution was also discussed, revealing that aragonite might be controlled by HMT molecules and NH_4^+ ions together.

© 2011 Elsevier Inc. All rights reserved.

1. Introduction

Calcium carbonate $(CaCO_3)$ has attracted considerable attention as it is not only one of the most abundant biomaterials in nature but also an important inorganic material with various industrial applications as filler in paper, rubber, plastics, and paints [1,2]. $CaCO_3$ often occurs as three anhydrous crystalline polymorphs such as calcite, aragonite, and vaterite [3]. Calcite is the most thermodynamically stable form of calcium carbonate under ambient conditions; the other two anhydrous crystalline forms are metastable in nature, with vaterite being particularly unstable [4]. Some biomimetic templates or additives such as Langmuir monolayers,[5] dynamic liquid–liquid interfaces [6], self-assembled monolayers [7], lipid bilayer stacks [8], vesicles [9], proteins extracted from $CaCO_3$-rich organisms [10] or synthetic molecules such as polymers [11,12] have been used for the synthesis of $CaCO_3$. More recently, Zhang et al. prepared $CaCO_3$ particles with different morphologies and polymorphs in the presence of p-aminobenzene sulfonic acid anhydrous-L-Lysine (L-Lys) complexes [13]. We have also synthesized $CaCO_3$ crystals with different morphologies using bacteria [14] and plant [15].

In biomineralization, polymorph selection is a key issue because different polymorphs offer the possibility of different materials properties. Excellent examples of polymorph control are found in organisms such as mollusks, which can selectively deposit aragonite, a specific polymorph of $CaCO_3$, under the control of biopolymers [16]. It has previously been reported that aragonite is formed in the presence of several extracted macromolecules from different shells in the presence [17] or absence [18] of an organic matrix, under compressed monolayers [19,20], at the liquid–liquid interface in a radial Hele–Shaw cell [6], by applying a double hydrophilic block copolymer [21], from the transformation of amorphous calcium carbonate nanoparticles in reverse surfactant microemulsions [22], by heat-induced precipitation onto self-assembled monolayers of anthracene-terminated thiol chains [7], or by high-power ultrasonic irradiation at certain sound amplitudes [23]. Yu et al. synthesized aragonite crystals in ethanol/water solution [24]. Our group obtained aragonite crystals in different Mg^{2+}/amino acid systems [25]. More recently, Gilbert showed that the N16N peptide self-assembled into layers and promoted aragonite growth in lamellar crystals [26].

To our knowledge, aragonite whiskers [27], sheaf bundles [21], fibers [28], tablets/films [29], needles [30], rods or spindles [23], thin-film [31], microspheres [32], etc. have been obtained by researchers. In this paper, the unusual dumbbell-flower-like aragonite superstructures were firstly synthesized using a low molecular weight organic-hexamethylenetetramine (HMT) as a modifier. One molecule

---

* Corresponding authors. Fax: +86 551 5108702.
E-mail addresses: s_yuhua@163.com (Y. Shen), anjx@163.com (A. Xie).

of hexamethylenetetramine has four six-atom loops. We chose the low molecular weight organic HMT with complex structure as a modifier to control the growth of CaCO$_3$ crystals, in order to simulate the biomineralization process. The aragonite crystals obtained may have applications such as using as a filler of functional polymers, etc. In general, the temperature of aragonite formation from a solution is above 40 °C [33]. Here, we found that aragonite superstructures were formed in HMT aqueous solution at room temperature. Very interestingly, the products transformed from calcite to vaterite primarily, and then changed into a mixture of aragonite and calcite with an increase of reaction time. The possible formation mechanism of aragonite in the presence of HMT was discussed. This study is very significant not only for synthesizing new and special functional materials, but also for providing new insights into biomineralization mechanism.

2. Experimental details

2.1. Materials and instruments

Anhydrous calcium chloride (CaCl$_2$), hexamethylenetetramine (C$_6$H$_{12}$N$_4$), ammonium carbonate ((NH$_4$)$_2$CO$_3$), and anhydrous ethanol were obtained commercially and were also analytically pure. All reagents above were used without further purification. Double-distilled water was used in all the experiments.

Fourier transform infrared spectroscopy (Nicolet 870, America) with a resolution of 4 cm^{-1} and a wave number range from 400 to 4000 cm^{-1} using the KBr pellet technique, X-ray diffractometer (DX-2000, Japan) using CuKα radiation at a scan rate of 0.06° 2θ S^{-1}, scanning electron microscopy (KYKY-EM3200, China; or Hitachi X-650, Japan) with an accelerating voltage of 18 or 20 kV were utilized to analyze our products. Transmission electron microscopy and selected area electron diffraction of the products were carried out on a JEM model 100SX electron microscope instrument (Japan Electron Co.) operated at an accelerating voltage at 200 kV. A conductivity meter (DDSJ-308, Shanghai, China) was also used.

2.2. Methods

2.2.1. Synthesis of CaCo$_3$ in different concentration of HMT aqueous solutions

First, seven groups of solutions were prepared (shown in Table 1). Then 50 mL of Solution 1 and the same volume of Solution 2 in every group were mixed completely, obtaining seven mixtures (marked as Mixture 1–7 orderly). Four beakers of Mixture 6 (containing 0.05 mol/L HMT and the same concentration of CaCl$_2$) and only one beaker of other mixtures each were prepared. Then above ten beakers containing the seven kinds of mixtures each were covered with PVC film, which was punched with four needle holes and placed in a larger desiccator. A small (50 mL) beaker containing 5.0 g of crushed ammonium carbonate solid was also covered with PVC film, punched with four holes, and placed at the

Table 1
Components of seven groups of reaction solutions.

Groups	Solution 1	Solution 2
1	Distilled water	0.01 mol/L CaCl$_2$
2	0.01 mol/L HMT	
3	0.1 mol/L HMT	
4	Distilled water	0.1 mol/L CaCl$_2$
5	0.02 mol/L HMT	
6	0.1 mol/L HMT	
7	0.5 mol/L HMT	

bottom of the desiccator. This desiccator was placed at room temperature (21–24 °C) for 7 days. In addition, when the reaction time reaches to 1, 2.5, and 48 h(s), a beaker containing mixture 6 was taken out for kinetics measurement (the precipitates were characterized).

The white precipitates produced in the above reaction solutions were separated from solutions by centrifugation (centrifugation rate, 4000 rpm), washed three times with double-distilled water and ethanol, and then vacuum dried for further determination.

The sizes and morphologies of the products were examined by scanning electron microscopy (SEM), while their components and crystal types were determined by Fourier transform infrared spectroscopy (FT-IR) and X-ray powder diffractometry (XRD) or selected area electron diffraction (SAED).

2.2.2. Conductivity measurement of CaCl$_2$ solutions before and after adding HMT

Conductivity of different aqueous solutions including 15 mL 0.05 mol/L HMT, 0.01 mol/L CaCl$_2$, and a mixed solution containing 0.05 mol/L HMT and 0.01 mol/L CaCl$_2$ was measured, respectively, for investigating the interaction between HMT molecules and Ca^{2+} ions.

3. Results and discussion

Fig. 1a–f shows the SEM images of CaCO$_3$ particles obtained from 0.005 mol/L CaCl$_2$ aqueous solutions containing different concentration of HMT after 7 days of reaction. From Fig. 1a, it may be seen that most of the particles obtained are rhombohedral without HMT. The enlarged image (Fig. 1b) shows that the particles are slippery with the length of diagonal from about 8 to 10 μm. Fig. 2a shows the FTIR spectrum of the as-prepared CaCO$_3$. Absorption bands centered at 874 and 712 cm^{-1} characteristic of the calcite phase of CaCO$_3$ are seen. The corresponding XRD pattern (Fig. 3a) of the CaCO$_3$ crystals displays the following diffraction peaks ($2\theta[°]$): 23.02°, 29.38°, 31.42°, 35.92°, 39.37°, 43.12°, 47.30°, and 48.49°, which can be correlated to the (hkl) indices (0 1 2), (1 0 4), (0 0 6), (1 1 0), (1 1 3), (2 0 2), (0 2 4), and (1 1 6), of calcite (JCPDS card number 72-1652). This is in agreement with the FTIR result.

When the mixed solution contains 0.005 mol/L HMT, two types of products can be seen (Fig. 1c and d). One is still rhombohedral, the size of which is close to that of those formed without HMT. The other is bunchy constructed from needle-like building units. The length of each "needle" is about 7–10 μm and the diameter of it is tens to hundreds nanometers. The diameter of the bundles is about 1–3 μm. It can be concluded that HMT molecules have an influence on the morphology of the products. The related FTIR spectrum shows that the characteristic peaks of the products are located at 874, 850, and 712 cm^{-1} (Fig. 2b), suggesting they are a mixture of aragonite and calcite. The intensity of the peak 850 cm^{-1} is stronger, implying that the higher content of aragonite in the products. The XRD pattern (Fig. 3b) of the as-prepared CaCO$_3$ crystals obtained displays the following diffraction peaks ($2\theta[°]$): 23.02°, 26.23°, 27.24°, 29.36°, 31.42°, 33.15°, 35.92°, 37.28°, 37.90°, 38.44°, 39.37°, 43.11°, 45.51°, 47.30°, and 48.49°, which can be correlated to the (hkl) indices (0 1 2), (1 0 4), (0 0 6), (1 1 0), (1 1 3), (2 0 2), (0 2 4), (1 1 6), of calcite (JCPDS card number 72-1652), and (1 1 1), (0 2 1), (0 1 2), (0 3 1), (1 1 2), (1 3 0), (0 4 0), of aragonite (JCPDS card number 76-0606). This is also in agreement with the FTIR result.

When the concentration of HMT in the reaction solution increases to 0.05 mol/L, novel dumbbell-flower-like CaCO$_3$ particles except for large portion of rhombohedral ones can be observed
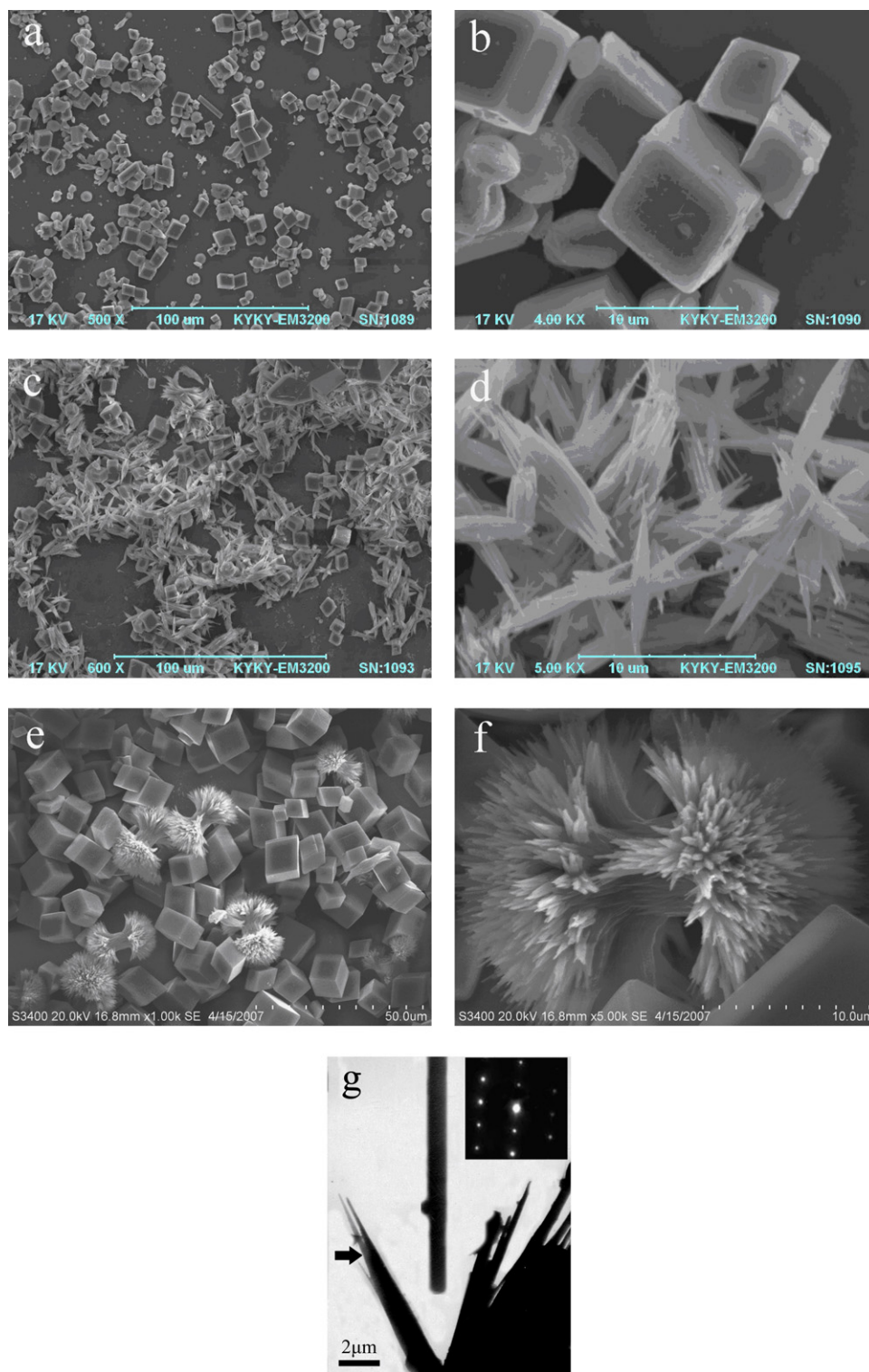
Fig. 1. (a–f) SEM images of CaCO$_3$ particles obtained in 0.005 mol/L CaCl$_2$ aqueous solution in the presence of different concentration of HMT after 7 days of reaction ((a, b): absence of HMT; (c, d): 0.005 mol/L HMT; (e, f): 0.05 mol/L HMT). In the images, (b), (d) and (f) are the magnified images of (a), (c) and (e), respectively. (g) TEM image and corresponding SAED pattern (top right corner) of needle-like portion of a dumbbell-flower-like CaCO$_3$ particle obtained in a mixed solution containing 0.005 mol/L CaCl$_2$ and 0.05 mol/L HMT.

(Fig. 1e and f). The length of the dumbbell-flower-like particles is about 20 μm. From the magnified image (Fig. 1f), it can be seen that the diameter of the "two head" is about 15 μm, and the length of the "middle stem" is about 5 μm. It also can be identified that the "dumbbell-flowers" are constructed from many small needle-like crystals with size of tens to hundreds nanometers. The

corresponding FTIR spectrum is shown in Fig. 2c, only obvious 874 and 712 cm^{-1} characteristic of the calcite phase can be seen. Related XRD pattern (Fig. 3c) shows that most of the diffraction peaks belong to calcite, but a weak peak located at $2\theta = 19.04°$ belong to aragonite. This suggests that the products contain a small quantity of aragonite crystals. Fig. 1g shows that the relevant TEM
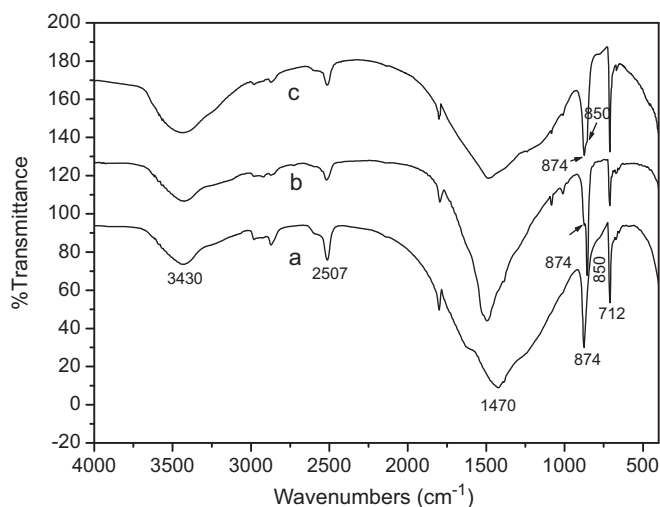
Fig. 2. FT-IR spectra of CaCO$_3$ crystals obtained in 0.005 mol/L CaCl$_2$ aqueous solution in the presence of different concentration of HMT after 7 days of reaction ((a): absence of HMT; (b): 0.005 mol/L HMT; (c): 0.05 mol/L HMT).
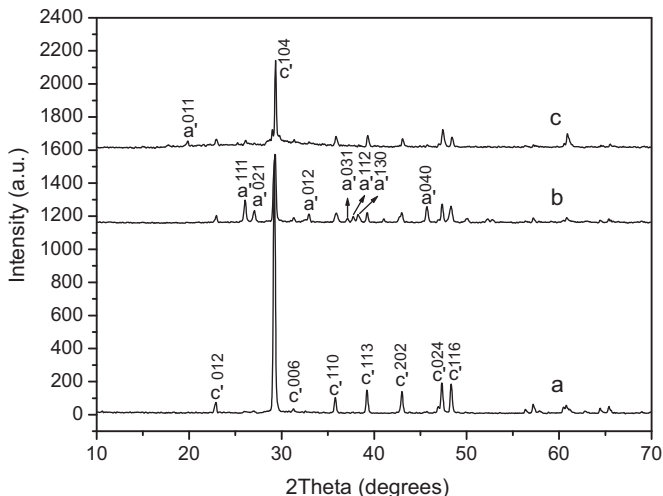

Fig. 3. XRD patterns of CaCO$_3$ crystals obtained in 0.005 mol/L CaCl$_2$ aqueous solution in the presence of different concentration of HMT after 7 days of reaction ((a): absence of HMT; (b): 0.005 mol/L HMT; (c): 0.05 mol/L HMT). In the patterns, a′ and c′ stand for aragonite and calcite, respectively.

image and SAED pattern of the needle-like portion of a dumbbell-flower-like particle, indicating that the "needles" are aragonite single crystals.

From the results above, it can be found that HMT may promote the formation of aragonite. We speculate that HMT molecules can influence the growth process of CaCO$_3$ crystals and be in favor of the aragonite formation.

In order to further investigate the influence of HMT on crystal growth of CaCO$_3$, we increased the concentration of CaCl$_2$ in the reaction mixtures. Fig. 4 shows the SEM or TEM images of CaCO$_3$ particles obtained in 0.05 mol/L CaCl$_2$ aqueous solutions in the presence of different concentration of HMT after 7 days of reaction. It can be seen that the CaCO$_3$ particles obtained are also rhombohedral in absence of HMT (Fig. 4a and b). But the size of them become larger than that of those formed in 0.005 mol/L CaCl$_2$ aqueous solution without HMT. The diagonal of them is from about 30 to 70 μm. The corresponding FTIR spectrum (Fig. 5a) and XRD pattern (Fig. 6a) both confirm the products are all calcite.

When the reaction mixture contains 0.01 mol/L HMT, part of the products changes from rhombohedral to quasi-spherical (Fig. 4c and d). The diameter of the quasi-spherical particles is about 2–3 μm. The enlarged image (Fig. 4e) shows that the surfaces of the products are rough. Related SAED pattern (at top right corner of Fig. 4f) suggests that they are calcite. This suggests that HMT molecules can control the shape and size of CaCO$_3$. In Fig. 5b, the related FTIR spectrum displays characteristic peaks of the calcite phase situated at 874 and 712 cm^{-1}, suggesting that the products are all calcite. The XRD pattern of these products shows that almost all of the diffraction peaks belong to calcite (Fig. 6b). If seen clearly, a weak peak located at $2\theta=19.04°$ appears, implying that the products contain a small quantity of aragonite.

As the concentration of the HMT is increased and becomes 0.05 mol/L in the reaction solution, two kinds of CaCO$_3$ are produced (Fig. 4g). One is also quasi-spherical with the diameter of about 1 μm. The other is bunchy constructed from needle-like building units. The magnified image (Fig. 4h) indicates that the diameter of each "needle" and the "bundle" is about 0.2–0.5 μm and 5 μm, respectively. Compared with those formed in Fig. 1c and d, it can be seen the "bundle" become more irregular. Here we speculate that lower concentration of Ca^{2+} may be in favor of the formation of regular aragonite superstructures. In Fig. 5c, the peaks situated at 874, 850, and 712 cm^{-1} can be observed, which confirms the products are a mixture of calcite and aragonite. The XRD pattern (Fig. 6c) of the as-prepared CaCO$_3$ crystals obtained displays the following diffraction peaks ($2\theta[°]$): 19.05, 23.02°, 26.23°, 27.24°, 29.36°, 32.62°, 35.92°, 45.92°, 47.30°, and 48.49°, which can be correlated to the ($h k l$) indices (0 1 2), (1 0 4), (1 1 0), (0 2 4), and (1 1 6), of calcite (JCPDS card number 72-1652), and (0 1 1), (1 1 1), (0 2 1), (1 2 1), and (221), of aragonite (JCPDS card number 76-0606). If I_C and I_V were defined as the intensity of the characteristic diffraction peaks of calcite from (1 0 4) and aragonite from (0 1 1), the value I_A/I_C may stand for the content of aragonite in the products. The value of I_A/I_C now is 0.13. Compared with that in Fig. 3c ($I_A^{011}/I_C^{104}=0.07$), it can be speculated that the content of aragonite in the products become higher with an increase of Ca^{2+} concentration in the same HMT solution.

When the concentration of HMT reaches to 0.25 mol/L, the CaCO$_3$ particles gained become smaller with rod-like shape (Fig. 4i and j). The length of the rods is about 2 μm, and the diameter of them is 0.5–1 μm. Some particles are congregated, showing complex morphologies. Absorption bands located at 874, 850, and 712 cm^{-1} in the corresponding FT-IR spectrum indicate that the products are a mixture of calcite and aragonite (Fig. 5d). In addition, the relative intensity of the peak at 850 cm^{-1} becomes stronger, suggesting that the content of aragonite in the products is increased. The XRD pattern of the products also shows the calcite and aragonite diffraction peaks (Fig. 6d). Obviously, the intensity of a peak at $2\theta=19.04°$ ((0 1 1) face of aragonite) becomes stronger ($I_A^{011}/I_C^{104}=0.37$), also suggesting that more aragonite is produced. This is in agreement with the FTIR result.

From the results above, it can be concluded that when the concentration of Ca^{2+} is 0.05 mol/L, the morphology of the products changes from spherical to needle-like or rod-like and the content of aragonite become increased with an increase of the concentration of HMT. We also can speculate that as to the same concentration of HMT, higher concentration of Ca^{2+} leads to higher content of aragonite in the products. If Figs. 1 and 4 are seen clearly, it can be found that lower concentration of Ca^{2+} is in favor of the formation of compact aragonite bundles.

In order to investigate the influence of aging time on the formation of CaCO$_3$ in the presence of HMT, SEM images (Fig. 7), FT-IR spectra (Fig. 8), and XRD patterns (Fig. 9) of the products
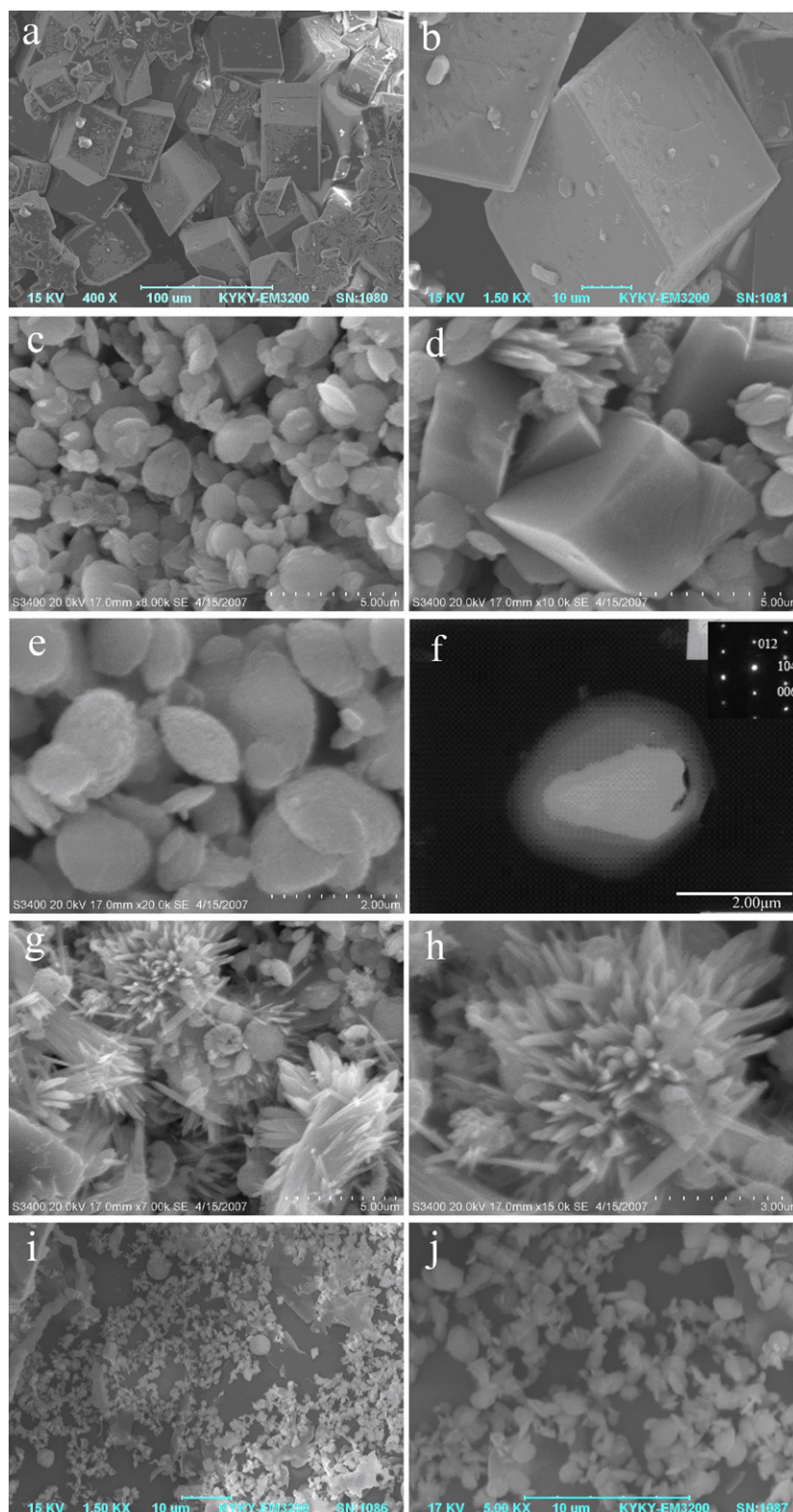
Fig. 4. (a–e, g–j) SEM images of $CaCO_3$ particles obtained in 0.05 mol/L $CaCl_2$ aqueous solution in the presence of different concentration of HMT after 7 days of reaction ((a, b): absence of HMT; (c–e): 0.01 mol/L HMT; (g, h): 0.05 mol/L HMT; (i, j): 0.25 mol/L HMT). In the images, (b), (d, e), (h) and (j) are the magnified images of (a), (c), (g) and (i), respectively. (d and e are magnified images of c.) (f) TEM image and corresponding SAED pattern (top right corner) of $CaCO_3$ particle obtained in a mixed solution containing 0.05 mol/L $CaCl_2$ and 0.01 mol/L HMT.

formed in the mixed solution containing 0.05 mol/L HMT and the same concentration of $CaCl_2$ at different reaction time were taken. From Fig. 7a and b, it can be seen that after 1 h of reaction, the $CaCO_3$ particles obtained are rhombohedral with the diagonal length of about 10 μm. When the reaction time reaches to 2.5 h, the morphology of $CaCO_3$ particles produced changes obviously. They become spherical with the diameter ranging from 2 to 7 μm (Fig. 7c and d). While after 48 h of reaction, most of the products
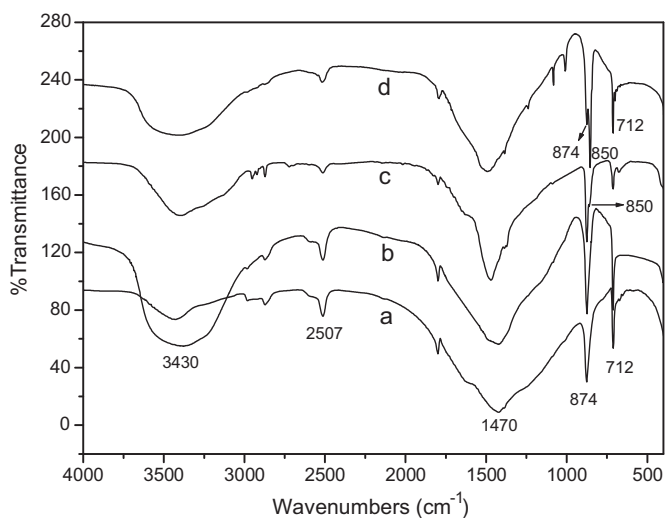
Fig. 5. FT-IR spectra of $CaCO_3$ crystals obtained in 0.05 mol/L $CaCl_2$ aqueous solution in the presence of different concentration of HMT after 7 days of reaction ((a): absence of HMT; (b): 0.01 mol/L HMT; (c): 0.05 mol/L HMT; (d): 0.25 mol/L HMT).
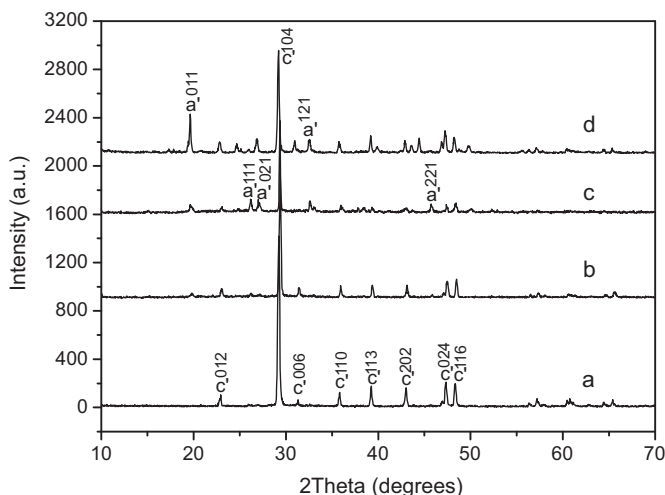

Fig. 6. XRD patterns of $CaCO_3$ crystals obtained in 0.05 mol/L $CaCl_2$ aqueous solution in the presence of different concentration of HMT after 7 days of reaction ((a): absence of HMT; (b): 0.01 mol/L HMT; (c): 0.05 mol/L HMT; (d): 0.25 mol/L HMT). In the patterns, a′ and c′ stand for aragonite and calcite, respectively.

become oval with diameter of about 2 μm (Fig. 7e and f). If seen carefully, it can be found that the surfaces of the particles are rough. From the results above, it may be found that the morphology of the $CaCO_3$ particles changes from rhombohedral to spherical and then to oval and the size of them becomes smaller with an increase of reaction time. We speculate that the $CaCO_3$ particles may undergo a part-dissolved process as the reaction time prolonged in the presence of HMT molecules. As shown in Fig. 4g and h, after 7 days of reaction, some of the particles become bundles constructed from needle-like building units.

Figs. 8 and 9 show the FTIR spectra and XRD patterns of $CaCO_3$ particles obtained at different reaction time. After 1 h of reaction (Fig. 8a), the $CaCO_3$ obtained show absorption bands at 874 and 712 cm^{-1}, indicating the products is calcite. The result of XRD pattern is in agreement with that of FTIR spectrum (Fig. 9a). After 2.5 h of reaction, absorption bands of the products in the FTIR spectrum are located at 874, 745, and 712 cm^{-1}, suggesting that the $CaCO_3$ crystals obtained are a mixture of calcite and vaterite. The XRD pattern (Fig. 9b) of the as-prepared $CaCO_3$ crystals

obtained displays the following diffraction peaks $(2\theta[°])$: 20.92°, 23.02°, 24.85°, 27.01°, 29.32°, 32.65°, 35.83°, 39.28°, 43.03°, 43.75°, 47.38°, 48.37°, and 49.90°, which can be correlated to the $(h\,k\,l)$ indices $(0\,1\,2)$, $(1\,0\,4)$, $(1\,1\,0)$, $(1\,1\,3)$, $(2\,0\,2)$, $(0\,2\,4)$, and $(1\,1\,6)$, of calcite (JCPDS card number 72-1652), and $(0\,0\,4)$, $(1\,1\,0)$, $(1\,1\,2)$, $(1\,1\,4)$, $(3\,0\,0)$, and $(1\,1\,8)$, of vaterite (JCPDS card number 72-1616), also suggesting that the products are a mixture of calcite and vaterite. If I_C and I_V are defined as the intensity of the characteristic diffraction peaks of calcite from $(1\,0\,4)$ and vaterite from $(1\,1\,0)$, the molar fraction of vaterite to calcite (X_V/X_C) can be calculated by the following equation [34]:

$$X_V/X_C = 7.691 I_V/I_C \qquad (1)$$

The content of vaterite in the mixture is about 64.9% (mol%) by this equation.

When the reaction time reaches to 48 h, the products change obviously identified from the FTIR and XRD results. Fig. 8c indicates the FTIR spectrum displaying the characteristic vaterite peaks located at 874 and 745 cm^{-1}. The intensity of the peak at 712 cm^{-1} is very weak. The related XRD pattern of the products shows they are also a mixture of calcite and vaterite, but the relative intensity of the diffraction peak $(1\,0\,4)$ decreases sharply (Fig. 9c). The content of vaterite calculated by the Eq. (1) is about 91.3% (mol%). After 7 days of reaction, the products change into a mixture of calcite and aragonite indicated by the FTIR and XRD results (Figs. 5c and 6c).

As discussed above, it can be seen that the $CaCO_3$ obtained in the presence of HMT molecules are transformed from stable calcite to unstable vaterite in the first stage. This process is abnormal and violates the Ostwald ripening [35]. It is probably due to the fact that the more and more NH_4^+ ions produced can stabilize the vaterite. In the second stage, the vaterite changes into a mixture of aragonite and calcite, and this is in agreement with the Ostwald rule of stages [35]. That is to say, the formation of aragonite undergoes an intermediate of vaterite in HMT aqueous solution.

In order to investigate the formation mechanism of aragonite induced by HMT, the electrical conductivity of HMT and $CaCl_2$ solution before and after adding HMT were monitored. Table 2 shows the electrical conductivity values of different solutions. It may be seen that the electrical conductivity of 0.01 mol/L $CaCl_2$ solution is 3100 μs/cm before it is mixed with 0.05 mol/L HMT, while it becomes 1700 μs/cm after the two solutions are mixed together. That is to say, it decreases to 1400 μs/cm. This suggests that a strong interaction takes place between HMT and Ca^{2+} ions, decreasing the transfer velocity of Ca^{2+} ions.

Fig. 10 shows the molecule structure of HMT. It can be seen that every HMT molecule contains four N atoms. These N atoms have lone pair electrons, which will make them complex with Ca^{2+} ions. The CO_3^{2-} ions produced by the decomposition of $(NH_4)_2CO_3$ then react with Ca^{2+} ions, forming $CaCO_3$ crystal nucleus adsorbed by HMT molecules. Aragonite is orthorhombic, the cell parameters of it are as follows: $a=0.495$ nm, $b=0.796$ nm, and $c=0.573$ nm. The distance between Ca and O atoms in Ca–O is 0.25 nm. HMT molecules may form aggregates through H bonds interaction, etc. When the aggregates of HMT molecules match the crystal lattice of aragonite, they may control the formation of aragonite crystals. From the XRD results (Figs. 3, 6 and 9), it can be seen that $(0\,1\,1)$ face of aragonite often appears. Here we speculate that HMT molecule aggregates may control the growth of aragonite crystals through absorbing onto their $(0\,1\,1)$ faces.

It is uncommon that calcite is transformed into vaterite with an increase of reaction time. Wu et al. reported that the abnormal structure conversion of $CaCO_3$ from calcite to vaterite by a supported liquid membrane containing a mobile carrier [36]. In their opinion, the interface of the oil and aqueous solution may be
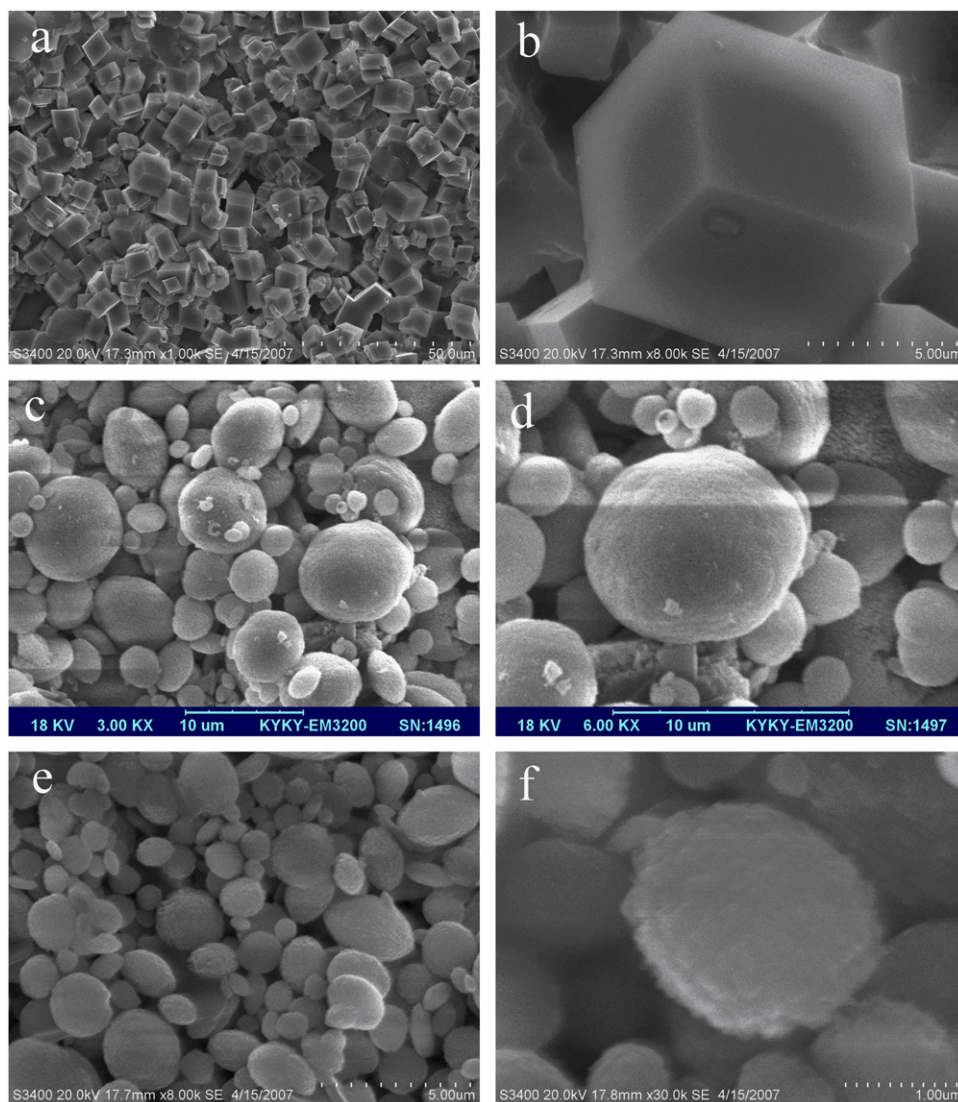
Fig. 7. SEM images of CaCO$_3$ particles obtained in a mixed aqueous solution containing 0.05 mol/L CaCl$_2$ and 0.05 mol/L HMT after different time of reaction ((a, b): 1 h; (c, d): 2.5 h; (e, f): 48 h). In the images, (b), (d) and (f) are the magnified images of (a), (c) and (e), respectively.
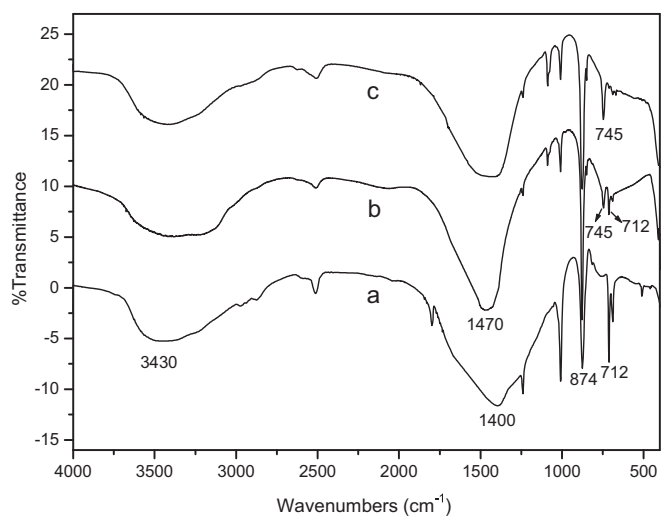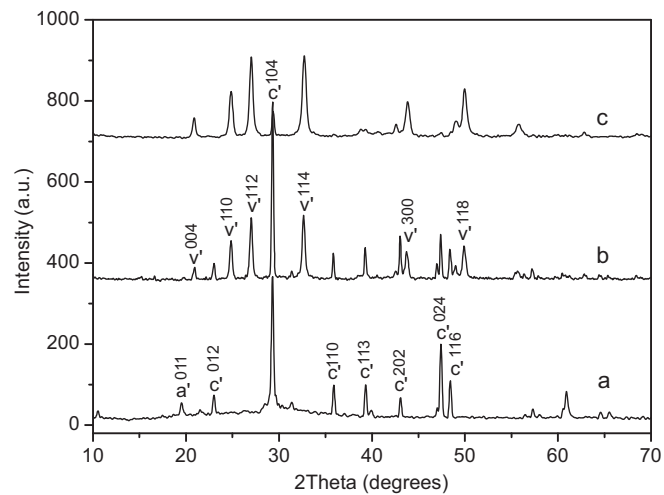

Fig. 8. FT-IR spectra of CaCO$_3$ crystals obtained in a mixed aqueous solution containing 0.05 mol/L CaCl$_2$ and 0.05 mol/L HMT after different time of reaction ((a): 1 h; (b): 2.5 h; (c): 48 h).

Fig. 9. XRD patterns of CaCO$_3$ crystals obtained in a mixed aqueous solution containing 0.05 mol/L CaCl$_2$ and 0.05 mol/L HMT after different time of reaction ((a): 1 h; (b): 2.5 h; (c): 48 h). In the patterns, v′, a′ and c′ stand for vaterite, aragonite and calcite, respectively.

Table 2
Conductivity of different aqueous solutions.

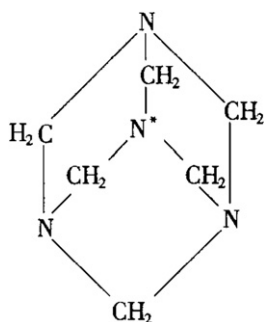| Solution	Conductivity
0.05 mol/L HMT	14 μs/cm
0.01 mol/L CaCl$_2$	3100 μs/cm
0.05 mol/L HMT+0.01 mol/L CaCl$_2$	1700 μs/cm

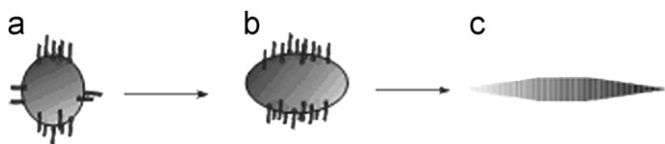**Fig. 10.** Molecule structure of HMT.

Fig. 11. Schematic representation of the growth process of aragonite crystals influenced by HMT.

unfavorable to calcite stabilization, leading to the dissolution of calcite in the beginning and the supersaturation of CaCO$_3$ in the reaction solution. The supersaturated solution of CaCO$_3$ benefits the growth of vaterite [37] which would adhere to the membrane wall spontaneously for decreasing their surface energy. In addition, the surface strength of the membrane may also stabilize the vaterite formed. The abnormal polymorph conversion of CaCO$_3$ from calcite to vaterite is controlled by the cooperation of supported liquid membrane system components. Helmut Cölfen found that NH$_4^+$ can help to form hexagonal vaterite within 18–40 h of reaction. After 3 days of reaction, hexagonal vaterite will change into rhombohedral calcite [38].

Here we think the formation mechanism of aragonite influenced by HMT and NH$_4^+$ ions may be as follows. In the beginning, calcite crystals are easy to form because of low concentration of NH$_4^+$ and low supersaturation of CaCO$_3$ in the reaction system. As the reaction time is increased, the concentration of NH$_4^+$ and the supersaturation of CaCO$_3$ become more and more high due to the constant decomposition of (NH$_4$)$_2$CO$_3$. Therefore, the condition may be in favor of the formation of vaterite and probable dissolution of calcite. The vaterite crystals with high energy may be stabilized shortly probably through adsorption of NH$_4^+$ onto their (1 1 2) and (1 1 4) faces (see Fig. 9b and c) [38]. Then oriented growth of the crystals adsorbed by HMT and NH$_4^+$ takes place (Fig. 11a), leading to their transformation from round to oval (Fig. 11b). As the reaction time is prolonged, more and more NH$_4^+$ ions are produced, which will make the crystals change into aragonite because of the stronger adsorption of NH$_4^+$ and HMT onto aragonite (0 1 1) faces. At last, needle-like aragonite crystals are formed (Fig. 11c), which may be stabilized by HMT and NH$_4^+$. HMT may form different aggregates in their different concentration, thereby leading to the different content of aragonite in the final products. In short, the formation of aragonite is probably due to the cooperation influence of NH$_4^+$ ions and HMT molecules. But the exact formation mechanism of aragonite in the presence of HMT needs further study.

4. Conclusions

Aragonite crystals with multilevel structures were synthesized using HMT as an additive and (NH$_4$)$_2$CO$_3$ as a CO$_2$ supplier. When the concentration of Ca^{2+} is 0.005 mol/L, the content of aragonite in products decreases with an increase of concentration HMT ranging from 0 to 0.05 mol/L, and the morphology of aragonite changes from bunchy to dumbbell-flower like. As the concentration of Ca^{2+} is increased and reaches to 0.05 mol/L and that of HMT ranges from 0 to 0.25 mol/L, the content of aragonite in products increases with an increase of HMT concentration. The morphology of the obtained aragonite transforms from rhombohedral to bunchy at first, and then into rod-like at last. The kinetic process of CaCO$_3$ formation in HMT aqueous solution is investigated, suggesting that the products transform from calcite to vaterite primarily, and then to a mixture of aragonite and calcite at last with an increase of reaction time. The formation mechanism of aragonite in HMT solution is discussed, which reveals that HMT molecules may control the growth of aragonite crystals probably through adsorbing onto (0 1 1) faces cooperating with NH$_4^+$ ions. It is very significant not only for the biomineralization research, but also for the synthesis of novel functional materials.

References

[1] E. Dalas, P. Klepetsanis, P.G. Koutsoukos, Langmuir 15 (1999) 8322–8327.
[2] M. Kitamura, J. Colloid Interf. Sci. 236 (2001) 318–327.
[3] L. Addadi, S. Raz, S. Weiner, Adv. Mater. 15 (2003) 959–970.
[4] H. Colfen, Curr. Opin. Colloid Interface Sci. 8 (2003) 23–31.
[5] E. Loste, E.D. Marti, A. Zarbakhsh, F.C. Meldrum, Langmuir 19 (2003) 2830–2837.
[6] D. Rautaray, A. Banpurkar, S.R. Sainkar, A.V. Limaye, N.R. Pavaskar, S.B. Ogale, M. Sastry, Adv. Mater. 15 (2003) 1273–1278.
[7] J. Kuther, G. Nelles, R. Seshadri, M. Schaub, H.J. Butt, W. Tremel, Chem. Eur. J. 4 (1998) 1834–1843.
[8] C. Damle, A. Kumar, M. Bhagwat, S.R. Sainkar, M. Sastry, Langmuir 18 (2002) 6075–6080.
[9] D. Walsh, S. Mann, Nature 377 (1995) 320–323.
[10] J. Aizenberg, D.A. Muller, J.L. Grazul, D.R. Hamman, Science 299 (2003) 1205–1208.
[11] L. Qi, J. Li, J. Ma, Adv. Mater. 14 (2002) 300–303.
[12] S.F. Chen, S.H. Yu, T.X. Wang, J. Jiang, H. Cölfen, B. Hu, B. Yu, Adv. Mater. 17 (2005) 1461–1465.
[13] Q. Zhang, L.Y. Ren, Y.H. Sheng, Y.T. Ji, J. Fu, Mater. Chem. Phys. 122 (2010) 156–163.
[14] L. Chen, Y.H. Shen, A.J. Xie, B. Huang, R. Jia, R.Y. Guo, W.Z. Tang, Cryst. Growth Des. 9 (2009) 743–754.
[15] L. Chen, Y.H. Shen, A.J. Xie, Q.N. Cheng, J. Mater. Sci. 45 (2010) 2938–2943.
[16] L. Addadi, D. Joester, F. Nudelman, S. Weiner, Chem. Eur. J. 12 (2006) 981–987.
[17] G. Falini, S. Albeck, S. Weiner, L. Addadi, Science 271 (1996) 67–72.

[18] A.M. Belcher, X.H. Wu, R.J. Christensen, P.K. Hansma, G.D. Stucky, D.E. Morse, Nature 381 (1996) 56–58.
[19] A.L. Litvin, S. Valiyaveettil, D.L. Kaplan, S. Mann, Adv. Mater. 9 (1997) 124–127.
[20] B.R. Heywood, S. Mann, Chem. Mater. 6 (1994) 311–318.
[21] N. Nassif, N. Gehrke, N. Pinna, N. Shirshova, K. Tauer, M. Antonietti, H. Cölfen, Angew. Chem. Int. Ed. 44 (2005) 6004–6009.
[22] L. Mei, B. Lebeau, S. Mann, Adv. Mater. 15 (2003) 2032–2035.
[23] G.-T. Zhou, J.C. Yu, X.-C. Wang, L.-Z. Zhang, New J. Chem. 28 (2004) 1027–1031.
[24] S.F. Chen, S.H. Yu, J. Jiang, F.Q. Li, Y.K. Liu, Chem. Mater. 18 (2006) 115–122.
[25] A.J. Xie, Y.H. Shen, X.Y. Li, Z.W. Yuan, L.G. Qiu, C.Y. Zhang, Y.F. Yang, Mater. Chem. Phys. 101 (2007) 87–92.
[26] R.A. Metzler, J.S. Evans, C.E. Killian, D. Zhou, T.H. Churchill, N.P. Appathurai, S.N. Coppersmith, P.U.P.A. Gilbert, J. Am. Chem. Soc. 132 (2010) 6329–6334.
[27] W. Wang, G. Wang, Y. Liu, C. Zheng, Y. Zhan, J. Mater. Chem. 11 (2001) 1752–1754.
[28] I. Sondi, B. Salopek-Sondi, S.D. Škapin, S. Šegota, I. Jurina, B. Vukelic, J. Colloid Interf. Sci. 354 (2011) 181–189.
[29] F.F. Amos, D.M. Sharbaugh, D.R. Talham, L.B. Gower, Langmuir 23 (2007) 1988–1994.
[30] L. Wang, I. Sondi, E. Matijevic, J. Colloid Interf. Sci. 218 (1999) 545–553.
[31] A. Sugawara, T. Kato, Chem. Commun. (2000) 487–488.
[32] W. Bao, H. Li, Y. Zhang, Cryst. Res. Technol. 44 (2009) 395–401.
[33] S.W. Lee, C.S. Choi, Cryst. Growth Des. 7 (2007) 1463–1468.
[34] A.J. Xie, Y.H. Shen, C.Y. Zhang, Z.W. Yuan, X.M. Zhu, Y.M. Yang, J. Cryst. Growth 285 (2005) 436–443.
[35] H. Cölfen, M. Antonietti, Langmuir 14 (1998) 582–589.
[36] Q.S. Wu, D.M. Sun, H.J. Liu, Cryst. Growth Des. 4 (2004) 717–720.
[37] N. Spanos, P.G. Koutsoukos, J. Phys. Chem. B 102 (1998) 6679–6684.
[38] N. Gehrke, H. Colfen, N. Pinna, M. Antonietti, N. Nassif, Cryst. Growth Des. 5 (2005) 1317–1319.